University of Groningen

Bachelor Thesis

Extraction of ions from a gas catcher

Author:
Leonardo Pome

Supervisors:
Julia Even
Beatriz Noheda

June 30, 2022

Abstract

Gas catchers are commonly used in the thermalization and extraction of nuclear reaction products. This is a fundamental process that readies the produced nuclei of interest for precision measurements. The aim of this work was to optimize the extraction of ions from a newly built gas catcher by studying the extraction of the decay products of a ^{223}Ra source. The extraction time and efficiency still needs to be improved as the ions of interest with relatively shorter half-lives were not successfully extracted. Further improvements on the electronics and on the gas-purity need to be implemented in the future.

This thesis was financially supported through NWO-natuurkunde Projectruimte grant (project number: 680-91-103).

Contents

1 Introduction **2**

2 Buffer gas chemistry **3**

3 Methods and setup **4**
3.1 Design of the gas catcher 5
3.1.1 Vacuum chamber and gas supply 5
3.1.2 Electrodes and Radio Frequency carpet 6
3.1.3 Foil and mesh for ion capture 8
3.2 Alpha spectroscopy and radioactive source preparation 9
3.2.1 Alpha spectroscopy and detection 9
3.2.2 Source preparation 10

4 Results and data analysis **12**

5 Discussion and conclusion **16**

References **19**

1 Introduction

Atomic nuclei in nature each have their own unique nuclear properties; these properties are strictly linked to the number of protons (Z, also referred to as atomic number) and neutrons (N) that each atom has. The proton and neutron number of a given nucleus can give insight into whether it will be stable or decay to reach an energetically feasible state. With the advancement of technology in the fields of nuclear chemistry and physics, research has found to be of essence to explore the possibilities offered by short-lived decaying nuclei that lie outside of the valley of stability, also referred to as *exotic nuclei*. Because of their instability exotic nuclei have only been studied and produced in controlled environments such as nuclear reactors and particle accelerators. The study of exotic nuclei will not only enrich the understanding of their properties but, will also provide background information and answers regarding the formation of chemical elements in our universe.

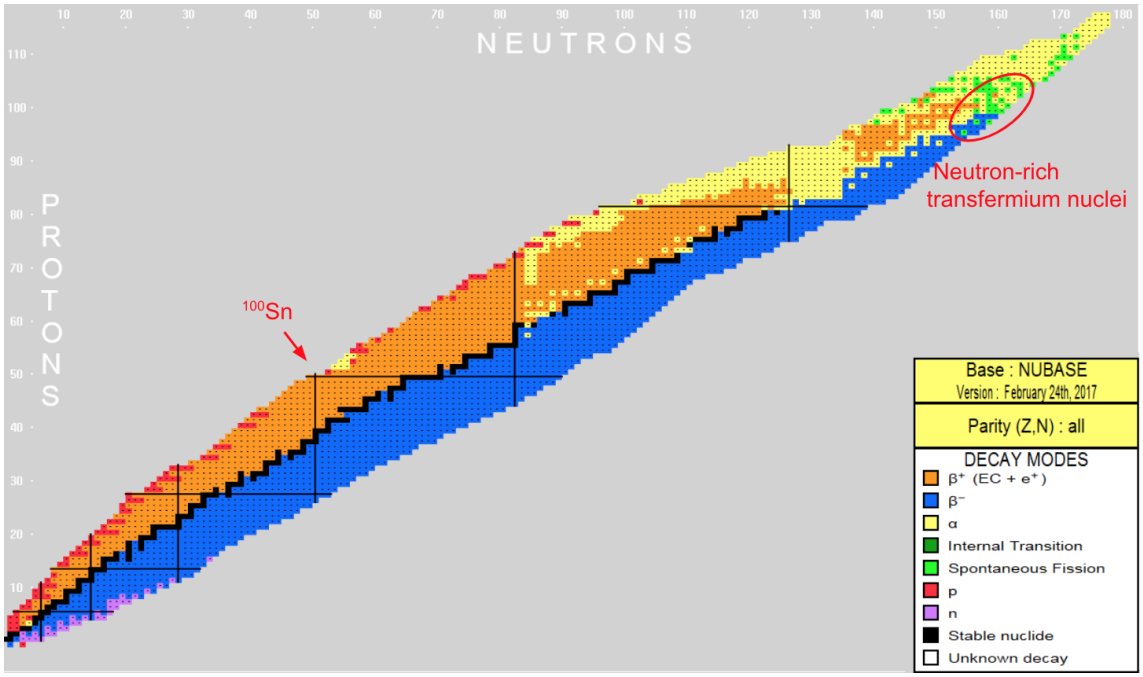

Figure 1: *The chart of nuclides contains all the known nuclei organized by neutron and proton number. The stable nuclei are labelled in black are surrounded by different species of radioactive nuclides. The black lines that cross the chart vertically and horizontally indicate proton and neutron shell closures (magic nuclei) [1]. The exotic nuclei relevant to this work are indicated on the chart.*

All the nuclei that have been discovered in nature and in nuclear experimental facilities have been compiled into the chart of nuclei (see Figure 1). In this chart, the different nuclei are organised by proton number (on y-axis) and neutron number (on x-axis). In this work, the exotic nuclei of interest lie at the extremes of nuclear stability: specifically the regions of neutron-rich transfermium elements (top right of Figure 1) and of neutron-deficient isotopes in the region of ^{100}Sn. In order to better understand the nuclear properties of these exotic nuclei, it is necessary to develop suitable and efficient experiments to allow for production, extraction and

direct mass measurements of the nuclides of interest. One of the biggest challenges in these experiments has been the low production yields and large amounts of unwanted by-products [1]. It is possible to remove non-isobaric by-products through an electromagnetic separator, though the unwanted isobars still remain. Furthermore, when the exotic nuclei are produced, they usually have energies that range from tens of MeV, for fusion evaporation reactions' products (^{100}Sn region), to hundreds of MeV, in case of nucleon transfer reactions and fragmentation reactions (transfermium region). Because these energies are too high to allow for low-energy high precision measurements, the energies of the exotic species of interest also need to be lowered. A novel technique is under development for the chemical separation of unwanted isobars from the ones of interest while also allowing for stopping and thermalizing high energy recoils through the use of a gas catcher device [2]. It is a device that slows down ions of exotic isotopes, produced in nuclear reactions, through the use of a gas; the gas atoms stop the ions as they collide, allowing the ions to go from highly charged states to extraction to low charges (+1, +2). The purity of the gas needs to be as high as possible to prevent the formation of molecules and charge-exchange reactions. For commissioning purposes the system is currently used with inert gasses; the gas catcher will later also be used with non-inert gas mixtures for chemical separations. In the framework of this study, the aim will be to investigate whether the ions produced by a alpha decaying ^{223}Ra are extracted efficiently from a gas-catcher device. The gas catcher device used in this study will then be used for high precision measurements in the CISE [2] and NEXT [3] projects.

2 Buffer gas chemistry

Nuclear reaction products can be thermalized in a buffer gas and then extracted for further study. In the process of thermalization, nuclear recoils are slowed down in the gas and a number of ion-electron pairs are formed. In gas stopping cells helium is typically used as buffer gas; in helium nuclear recoils tend to remain ionized because helium's first ionization potential is the largest of any element. When a radioactive source, such as ^{223}Ra, is introduced inside a gas cell, the buffer gas will be ionized by the alpha particles emitted by the source's radioactive decay. After being ionized the gas ions will rapidly undergo dimerization, in what is known as a thermonuclear reaction. The thermonuclear dimerization reaction for helium is known to have the following chemical equation [4]:

$$He^+ + He + He \rightarrow He_2^+ + He \tag{1}$$

According to Morrissey et al. "all of the primary ionization caused by the nuclear recoils will be converted into He_2^+ ions within a timescale that is short compared to the extraction time of those recoils from any gas cell"[5]. Impurities constitute a big obstacle for nuclear recoils to remain preferentially ionized: compared to helium, even small amounts of contaminants can become the dominant charge carriers through charge transfer reactions. Two of the most common impurities in gas catchers are water and nitrogen: these impurities will tend to attract the charges and will thus in turn also be ionized. The impurities are usually either ionized via a bimolecular

reaction with a helium dimer ion or a trimolecular reaction with an extra helium atom (where IM can either be an impurity molecule or an atom):

$$He_2^+ + IM \rightarrow IM^+ + 2He \tag{2}$$

$$He_2^+ + IM + He \rightarrow IM^+ + 3He \tag{3}$$

The ions of interest are expected to be extracted only if the impurities are very low and the drift time in the gas cell is also short. It is possible to reduce contaminants to a few parts per billion from a gas cell with helium purifiers and ultra-high-vacuum (UHV) conditions. The uniform gas purity level obtained using helium purification techniques, in of itself might also not guarantee a uniform charge transfer reaction from the helium dimer ion (He_2^+); this is due to the fact that a higher pressure lowers also the ions ability to move, as well as increasing drift time and molecular collisions that might lead to charge transfers or molecule formation [5].

3 Methods and setup

The CISe (chemical isobaric separation) is a novel setup that consists of three main parts (as shown in Figure 2): a gas catcher is connected to a quadruple Time-of-flight spectrometer (QTof) through an ion guide. In this study, only the gas catcher has been used. The first hexapole has been replaced by a ORTEC 19754C detector with in front a aluminium mesh, to investigate whether the ions are being captured and guided through to the spectrometer properly.

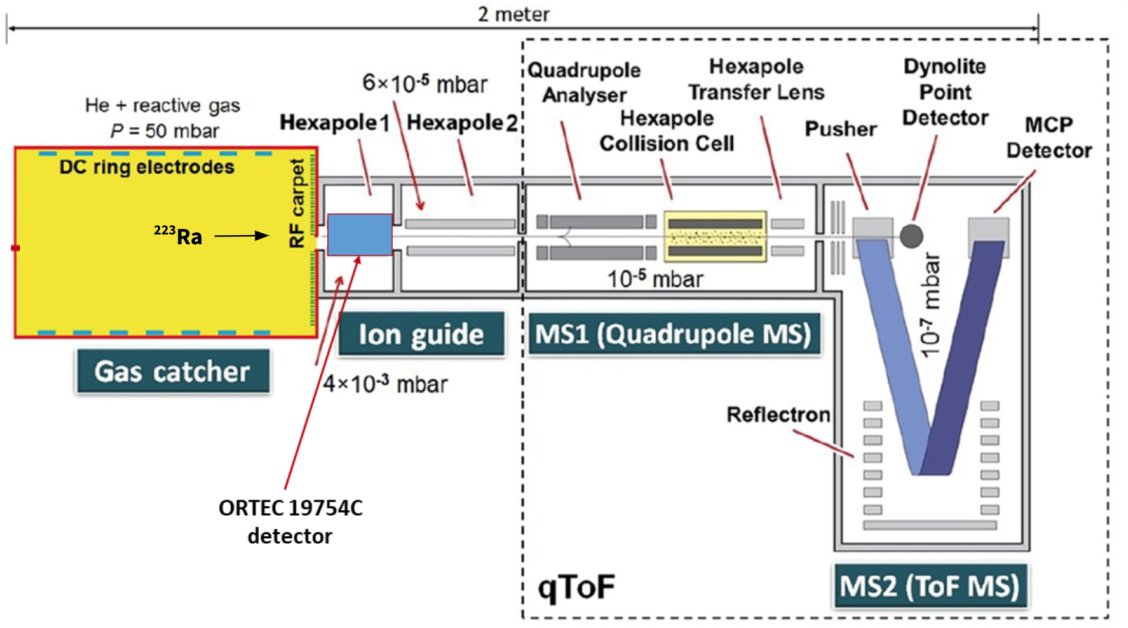

Figure 2: *Schematics of the setup showing gas catcher connected through QTof via ion guide (consisting of hexapole 1 and 2) [2].*

3.1 Design of the gas catcher

Gas catchers are used to slow down and prepare ions for low-energy, high-precision measurements. The gas catcher used in this setup is a vacuum chamber (kept under vacuum through a high vacuum system), that houses a gas supply apparatus and an electrode system. The electrode system comprises of a cage with DC electrodes and one RF carpet. The ions are introduced in the system by placing a alpha decaying ^{223}Ra radioactive source onto the target holder closest to the RF carpet. The different components can be seen in Figure 3 and will be described in more depth in the following sections. [6].

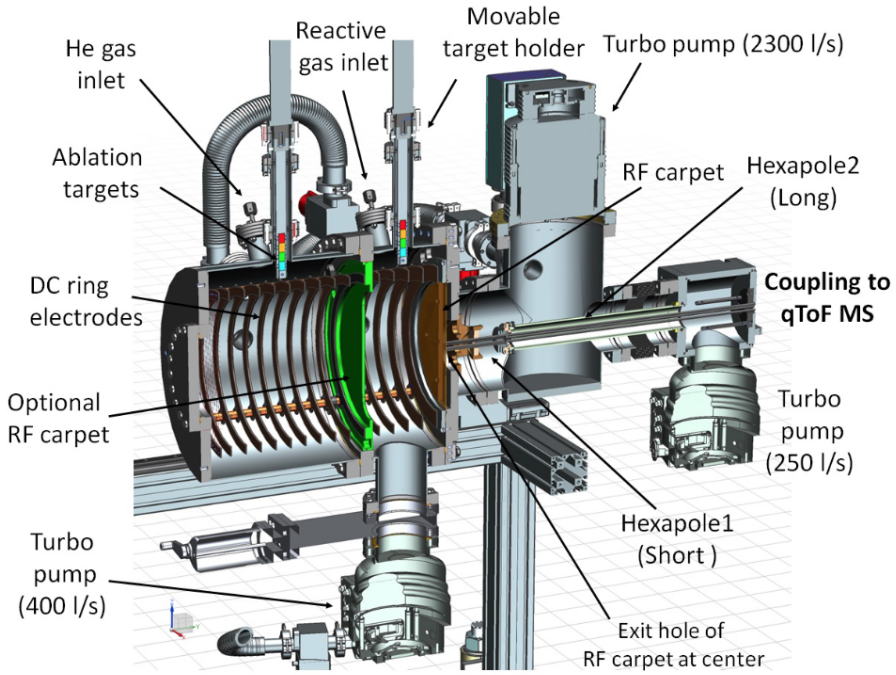

Figure 3: *Technical view of the gas catcher coupled to the ion guide [2].*

3.1.1 Vacuum chamber and gas supply

The vacuum chamber has been built with the setup at SHIPTRAP in mind [7]; its size has been optimized in order to be able to most efficiently stop distribution of the fusion-evaporation residues in the region around atomic number 100. Various simulations with different ion energies, helium pressures and entrance window thickness have been performed in order to establish the size of the different components within the gas cell. The chamber's diameter is 400 mm and is 450 mm long. It has been designed to be able to be sectioned into two adjacent compartments: a 150 mm reaction chamber and a 300 mm stopping chamber. The cell is made of stainless steel and and is made up of ConFlat flanges to ensure Ultra-High vacuum conditions. The different flanges have been hosted with electrical troughs for measuring equipment, various connections to vacuum pumps and gas inlets for different gasses. A Leybold TURBOVAC 450i and MAG W 2200 iP turbo-molecular pumps allow for high vacuum conditions inside the cell to take place: the vacuum conditions are

measured through sensors placed inside the cell and can be read both on a digital pressure monitor (the pressure monitor is not set up to measure helium pressures but can still be used to check on the status of the cell while operating the setup) and an analog pressure gauge. The cell is operated at room temperature (T= 293 K) and at a helium pressure of 50 mbar. In order to operate the CISE gas catcher successfully the chemical reagent needs to be introduced in high purity helium (5.6 or 6.0, ideally). The cell is connected to two stainless steel gas lines with a diameter of 6 mm (see Figure 3). The gas flow of helium into the gas cell is manually controlled through a valve.

3.1.2 Electrodes and Radio Frequency carpet

The DC electrodes inside the CISe gas catcher are used to guide ions; the RF and DC fields on the carpet and help with the focal extraction of ions from the gas catcher into the ion guide. A DC gradient is created applying a maximum voltage (DC max) to the grid electrode and a minimum voltage (DC min) to the last electrode (the one close to the carpet). To further create a potential gradient, in between each electrode lies a 50 kΩ resistor. Three different high-voltage power supplies (manufactured by iseg with max output of 4kV) are used to supply both the DC electrodes on the cage and on the carpet. As seen in Figure 4, the first electrode supports a grid with a 1x1 cm wire mesh: this allows for ions to be guided along the length of the gas catcher towards the carpet. The first 13 electrodes starting from the grid are all 280 mm; the last 3 are progressively smaller in order for the last one to match the diameter size of the RF carpet (250 mm). The electrodes are connected to one another and to the flange that holds the carpet via four support rods. The ion trajectories moving down the DC gradient created by the electrode cage can be seen in Figure 5.

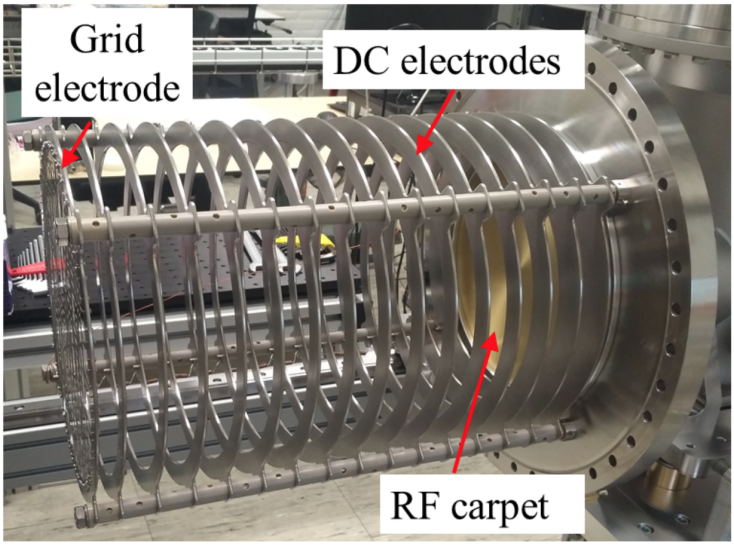

Figure 4: *Cage made up DC ring electrodes and a grid electrode. RF carpet is in front of the hexapoles on the extraction side of the gas cell [1].*

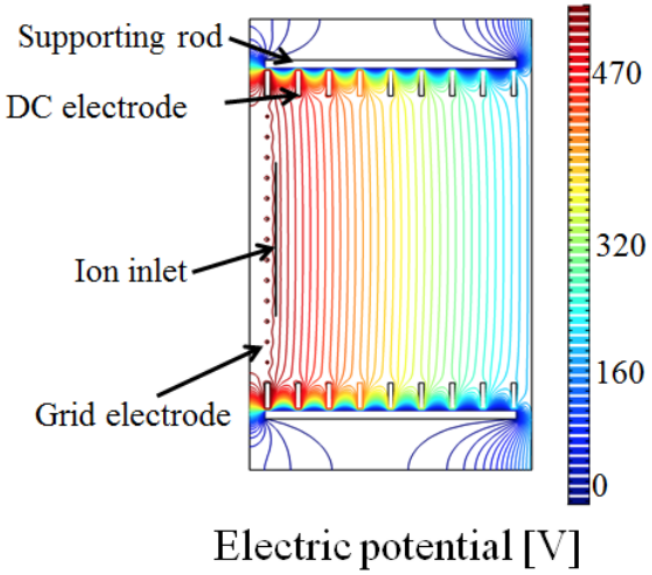

Figure 5: *The simulated potential gradient created by the DC electrodes is shown (Figure adapted from [1])*

Mounted at the extraction side of the gas cell can be found the RF carpet; the carpet consists of a printed circuit board with 500 concentric rings of electrodes. The outer diameter of the carpet is 280 mm whereas the inner one is 250 mm. There is a 0.45 mm exit hole for the ions to be extracted (in the case of this investigation, to the detector) in the center of the carpet. The backside of the carpet holds the electronics needed for the carpet to function properly. The pressure difference between the gas cell and the ion guide creates a powerful gas-jet. The gas-jet and the alternating (π) RF voltage applied to the consequent ring electrodes favour a funneling effect that allows for the ions to concentrate and go through the exit hole (see Figure 6).

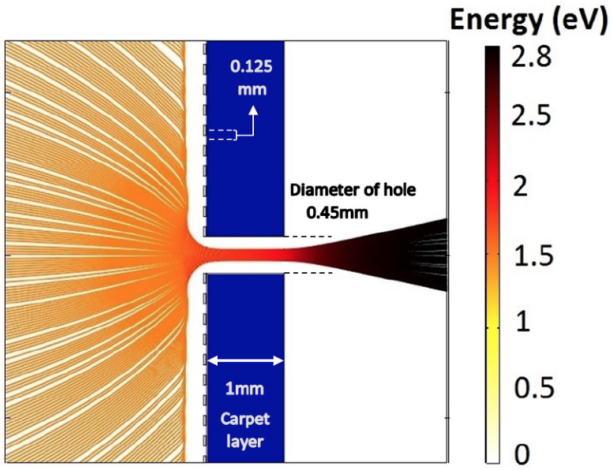

Figure 6: *Viscous-drag model simulation of the ion trajectories close to the exit hole of the carpet. Both gas flow and DC and RF fields are taken into account in the simulation, as well as collisions between helium and the ions of interest [2].*

3.1.3 Foil and mesh for ion capture

Behind the carpet, the first hexapole of the ion guide has been taken out and replaced by the detector as show in Figure 7. The detector is housed in a thermoplastic polymer support made out of PEEK (polyether ether ketone); the detector holder is placed 15 mm behind a mesh holder (also made out of PEEK) (see Figure 8). A variation of the mesh holder has been used in the past to also hold metal foils (Mylar and aluminium foil, as well as aluminium and stainless steel meshes). The mesh or foil holder lies $\sim$ 8.75 mm behind the exit hole of the carpet. The current setup uses an aluminium mesh with $\sim$ 1.5 mm holes and wire thickness of 0.3 mm. The mesh is responsible for catching the ions that are extracted through the carpet: negative voltages are applied onto the mesh in order to trap the positive ions coming through the exit hole. The ions caught onto the mesh are then to decay and expected to hit the detector that sits right behind the mesh.

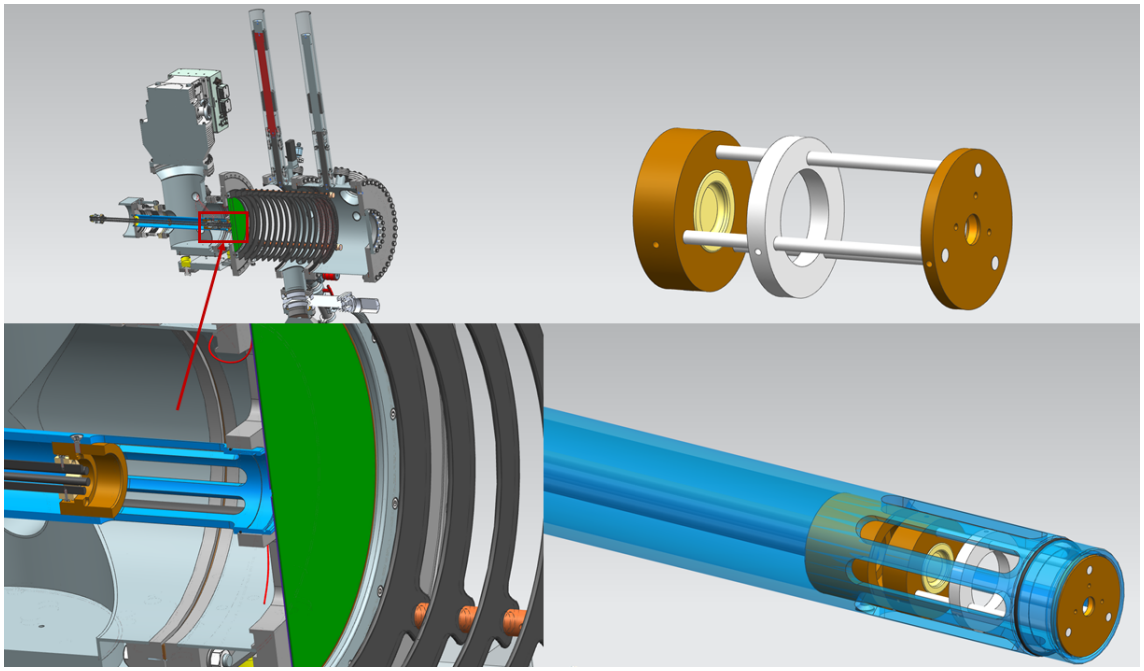

Figure 7: *Top left: whole gas cell is shown, the section that houses the detector (previously housing hexapole 1) is shown behind carpet highlighted in red. Bottom left: hexapole 1 has been taken out of blue guide. Top right: ORTEC 19754C detector is placed 1.5 cm behind the mesh/foil holder. Bottom right: Detector placed inside the hexapole guide.*

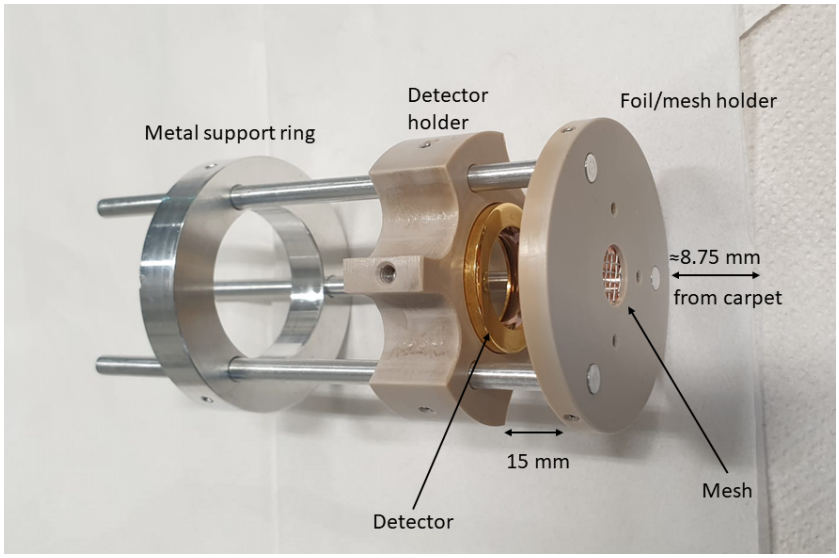

Figure 8: *The detector holder and mesh/foil holder are mounted on three rods supported by a metal ring.*

3.2 Alpha spectroscopy and radioactive source preparation

3.2.1 Alpha spectroscopy and detection

Alpha particles have high energies between 4 and 9 MeV. Due to their high energy, alpha particles cause intense ionization. In order to measure alpha particle emission, silicon detectors are used. There are two types of detectors used for alpha spectroscopy: surface barrier detectors (or SBB) and passivated ion-implanted detectors (or PIPS) [8]. The experimental setup uses a ORTEC 19754C (shown top right in Figure 7) which is a surface barrier detector. In order for the detector to work the sample has to be placed in front of the detector or close to it (see Figure 3, the sample is placed onto the target holder closest to carpet). Both sample and detector need to be under vacuum to avoid absorption of alpha particles in the surrounding environment. A bias voltage is applied on the detector: different bias voltages will lead to different count resolution. The detector creates pulses that are then amplified by first a pre-amplifier and then subsequently by a linear amplifier (see Figure 10). The analog pulses from the detector are converted into digital signals using a ADC (analog-to-digital-converter). Once converted into digital signals, a MCA (multi channel analyzer) will determine the height of the counts corresponding to different channels. Counts per channel can then be converted into counts per energy (see Figure 9).

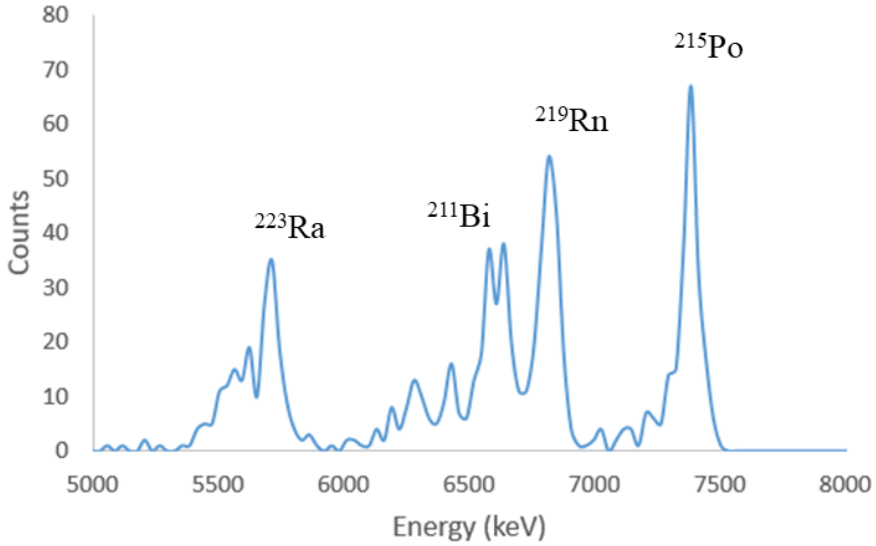

Figure 9: *Typical non-fitted alpha spectrum obtained by placing the radioactive source close to the detector and applying a 70 V bias voltage on the detector and -2500 V on the aluminium mesh that lies in front of the detector. The various peaks indicate radium (^{223}Ra), polonium (^{215}Po), bismuth (^{211}Bi) and radon(^{219}Rn) and are being counted by the detector (see Figure 12 for decay chain of radium starting from actinium).*

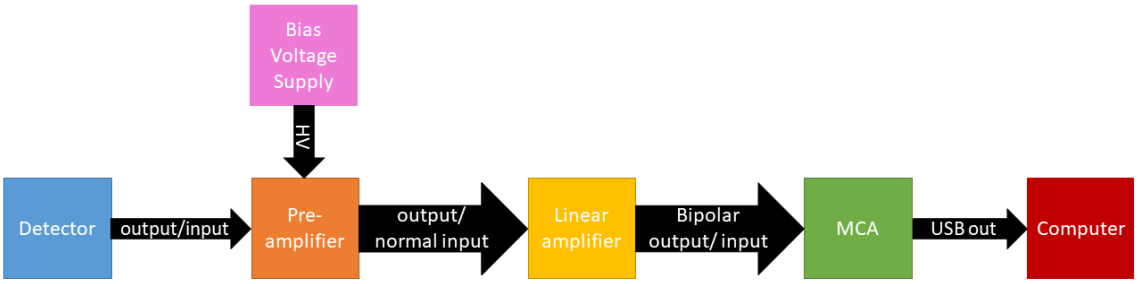

Figure 10: *Schematic of the detection electronics*

3.2.2 Source preparation

A radium source was chosen for this investigation. The ^{223}Ra isotope has a well known easily identifiable decay chain (see Figure 12) and because it decays into radon, which has a half life of around 4 s, it is possible to tell whether the ions are being efficiently extracted in a short amount of time. The ^{223}Ra source is prepared starting from an open ^{227}Ac source. The details concerning the decay of actinium can be seen in the decay chain illustrated in Figure 12. A schematic view of the setup used for source preparation is shown in Figure 11 [9]. The actinium source is positioned at the bottom of a cell filled with 30 mbar of helium gas. A screw on which a negative voltage (-300 V) is applied, is placed a couple of centimeters above the ^{227}Ac source. ^{223}Ra ions will recoil from the actinium source after alpha-decaying of thorium (^{227}Th). ^{223}Ra ions will then be stopped in the helium gas and

transported onto the screw, attracted by the negative potential on the screw. In order to make sure that only the tip of the screw receives the radium ions, a metal tube is used to cover the sides and top side opposite the actinium source.

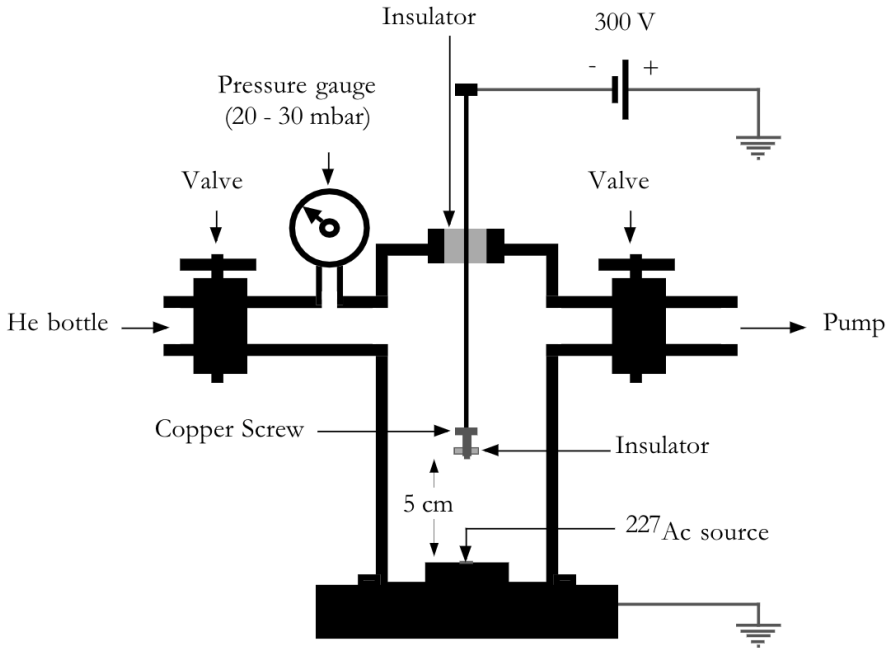

Figure 11: *Schematics of the setup used for source preparation [9]*

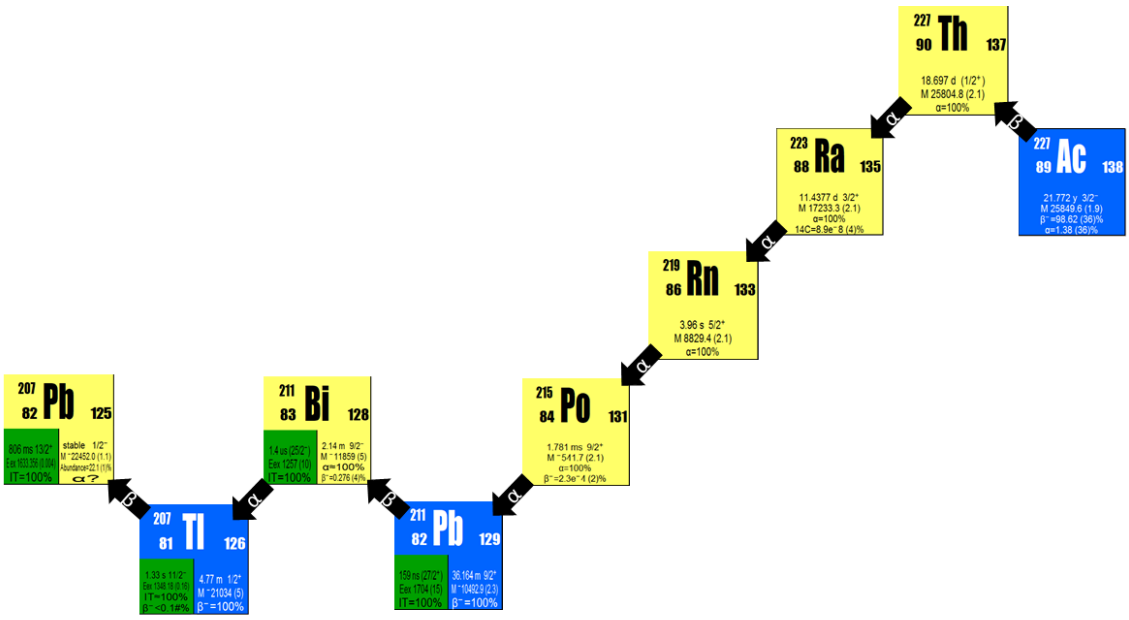

Figure 12: *The source is prepared starting from actinium and will decay to stable lead via radium, radon, polonium and bismuth. The decay modes are indicated (yellow alpha decay, blue beta decay) as well as the half-lives.[10]*

4 Results and data analysis

Before starting the investigation, the detector was tested in order to see if it was working properly. A series of measurements was conducted in which the source screw was placed in front of the mesh and detector. The radioactive screw was mounted in the center of a circular stainless steel plate of the same diameter of the carpet; the carpet was then replaced by the source plate, thus allowing the radioactive tip of the screw to face the detector (placed in the ion guide). Different bias voltages were applied onto the detector to establish the voltage that would give the alpha spectrum with the highest resolution. A bias voltage of 70 V was found to be the optimum. The alpha spectrum is shown in Figure 13. The data for this alpha spectrum was calibrated and fitted in order to see if the energy of the measured peaks corresponded to the expected energy of the ions (expected values for the energies are taken from [11]). The results are compiled in Table 1.

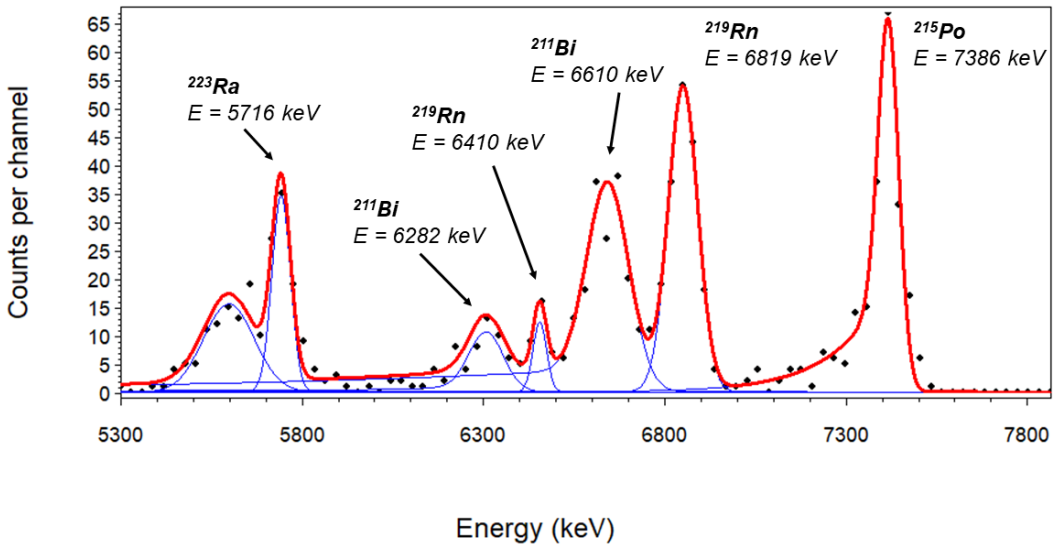

Figure 13: *Calibrated and fitted alpha spectrum of the ^{223}Ra placed in front of the detector with 70 V bias voltage.*

Table 1: *Expected and measured energies for the decaying ions. [11]*

Ion	Measured Energy (keV)	Expected Energy (keV)
^{215}Po	7386	7386
^{219}Rn	6819	6819
^{211}Bi	6610	6622
^{219}Rn	6410	6425
^{211}Bi	6282	6278
^{223}Ra	5716	5716

Following the source plate measurements, the carpet was put back in place and the source screw was placed onto the target holder closest to the carpet ($\approx$ 7.5 cm). In all the carpet measurements, because now the source is placed in helium the ^{223}Ra

peaks are not expected to be measured as the radium decays in the gas cell. In order to investigate whether the ions are guided through the carpet successfully a series of measurements was made. In the first of these measurements, a voltage of $-3000\,\mathrm{V}$ was applied on the mesh and all the electronics were turned on (electrode cage = $250\,\mathrm{V}$, carpet = $125\,\mathrm{V}$, target holder = $80\,\mathrm{V}$, RF voltage = 75 V_{pp}; 91 V_{pp}). The result of the measurement is shown in Figure 14. The spectrum's energy calibration was made using the same calibration derived from the source plate measurement shown in Figure 13. The peaks are shown to have energies of 6621.4 keV and 6278.5 keV respectively: these values coincide with the literature values for the ^{211}Bi peaks (see Table 1)[11]. The counts at lower energy can be attributed to statistical fluctuations and noise.

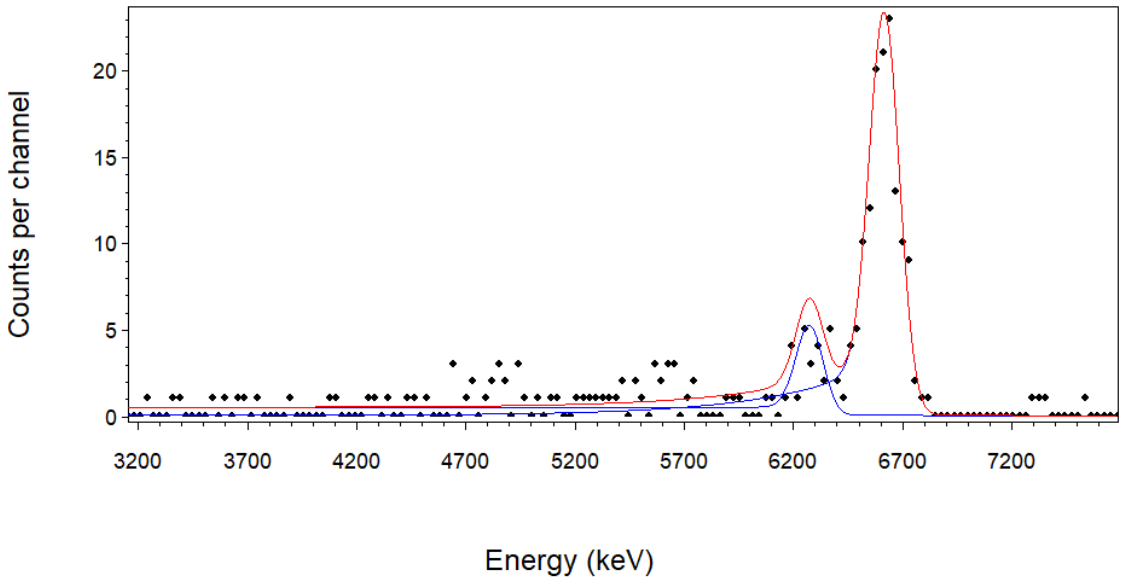

Figure 14: *Calibrated and fitted alpha spectrum of a measurement made with the following settings: mesh = -3000 V, electrode cage = 250 V, carpet = 125 V, target holder = 80 V, gas cell pressure = 20 mbar, detector bias voltage = 70 V, RF voltage = 75 V_{pp}; 91 V_{pp}. Peak energies coincide with bismuth (6621.4 keV; 6278.5 keV).*

If the ions are guided properly past the carpet, once the carpet and DC electrode cage are turned off, they will be attracted by the negative potential on the mesh. These ions will then decay in time off of the mesh and hit the detector. To check this, in the next measurements the target holder with the source was retracted from the gas cell and the electronics were turned off. This is done to prevent more ions from being accumulated onto the mesh, thus allowing to make sure that the only ions hitting the detector are decaying off of the mesh. To check whether what is being accumulated is effectively bismuth, it is possible to calculate the half-life from plotting the activity against the time elapsed.

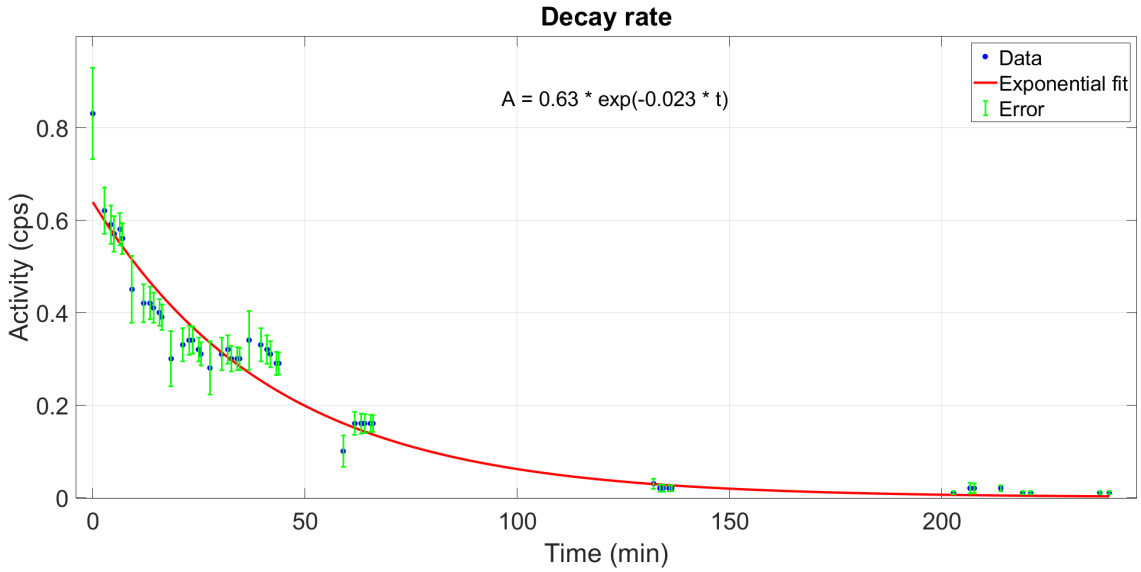

Figure 15: *Decay rate is plotted by measuring activity at different times. The graph was fitted using an exponential function and the equation for the trendline is indicated on the Figure.*

The decay constant (λ) can then be extrapolated from the plot by applying an exponential fit to the data points. The exponential fit equation is related to the radioactive decay law:

$$A = A_0 \cdot e^{-\lambda t} \tag{4}$$

As shown in Figure 15 the decay constant, (λ) = 0.0215; from this the half life can be calculated knowing that:

$$\lambda = \frac{ln2}{t_{\frac{1}{2}}} \tag{5}$$

thus;

$$t_{\frac{1}{2}} = \frac{ln2}{0.023} = 30.1 \text{ minutes} \tag{6}$$

The literature value for the half life of bismuth is 2.14 minutes which is very different from the calculated value of 30.1 minutes. This result is much closer to the value for the half life of lead instead, which has a half life of 36 minutes. It can be seen in the plot that the first data point is not part of the exponential fit of the data. This has been done on purpose as it has been a constant for the activity at the beginning of every measurement to be decaying with a much faster decay rate than the measured decay after a 10 minutes of measurement time. In order to visualize this the decay of ^{211}Bi ($t_{\frac{1}{2}}$ = 2.14 min) and ^{211}Pb ($t_{\frac{1}{2}}$ = 36.1 min) was calculated using the radioactive decay law (Equation 4, where A_0 is the same starting activity of the measurements) and plotted over the same time interval. In Figure 16, the calculated activity of ^{211}Bi decaying is shown in pink and the calculated activity of ^{211}Pb is shown in black.

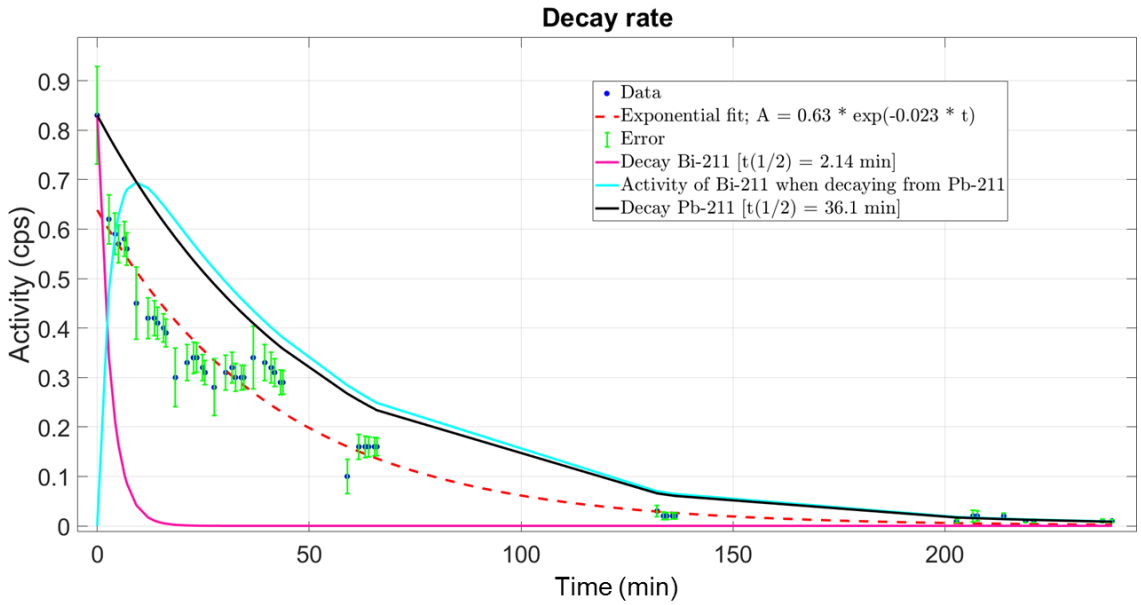

Figure 16: *The exponential fit function for the decay rate observed in experiment is plotted alongside: decay of ^{211}Bi using Equation 4 (pink line), decay of ^{211}Pb using Equation 4 (black line),^{211}Bi's activity calculated from consecutive decay of ^{211}Pb (light blue line).*

In Figure 16, can be seen that from the first data point to the second there is a relatively steep drop in activity. This drop in activity is consistent with the decay of ^{211}Bi plotted in pink. After a few ^{211}Bi half lives the measured decay rate trendline (dashed red line) starts to resemble that of the decay of ^{211}Pb (plotted in black). This supports the idea that both lead and bismuth are getting caught onto the mesh; after a while the initially accumulated bismuth will be still decaying but it will exhibit much lower activity. In time the decay of lead will replenish bismuth (shown in light blue) which will then in turn decay and hit the detector. The observed half life will then be closer to that of lead for the remainder of the measurement.
When the electronics remain on from one measurement to the next the background counts that remain from the previous measurement need to be accounted for. The radioactive decay law (see Formula 4) can be used again to calculate the decay activity after time t. In the next measurements the residual activity from previous measurements was tabulated:

Table 2: *Time elapsed between every measurement is tabulated along the residual activity from one measurement to the next and the average counts per second recorded over the whole measurement.*

Measurement	Time (s)	Total counts (cps)	$A_{residual,Pb}$ (cps)	$A_{residual,Bi}$ (cps)
1	4500	0.179	0.042	$2.65 \cdot 10^{-13}$
2	1800	0.154	0.086	$9.32 \cdot 10^{-6}$
3	3600	0.101	0.031	$3.67 \cdot 10^{-10}$
4	1800	0.162	0.091	$5.7 \cdot 10^{-10}$

To calculate how many counts come from what has been accumulated on the mesh we need to subtract the calculated residual counts from the previous measurement from the total number of counts. An example of this calculation is as follows:

$$cps_{mesh} = M2_{cps} - (A_{M1\ residual}) = 0.179 - 0.042 = 0.137 \text{ cps} \tag{7}$$

where M2 is the total counts from measurement 2 and $A_{M1\ residual}$ is the residual activity from measurement 1. From the Table 2 it can be seen the counts from the bismuth decay are negligible after more than 1800 seconds. Most residual counts come from the lead decaying into bismuth. If the lead counts are subtracted, as shown in Equation 7, counts are still present. From this, as well as looking at the results obtained by plotting the decay rate (see Figure 16), it is possible to further support the idea that ions are being caught onto the mesh as lead and then decay onto the detector as bismuth.

5 Discussion and conclusion

From the data gathered it is possible to infer that lead and bismuth are being extracted from the gas catcher device. This result does not come without some considerations and the acknowledgement of some limitations. It was initially expected that ^{219}Rn and ^{215}Po would also be extracted. However, neither the alpha decay of ^{219}Rn nor of ^{215}Po has been observed in the spectra. Only two bismuth peaks were found to be present (as seen in Figure 14). This result hints at the fact that the extraction is either too slow or the purity of the gas inside the gas catcher is too low, for polonium and radon to be efficiently extracted (or a combination of the two reasons). In the first case, it would mean that there is something hindering the transmission of the ions through to the detector once the carpet is used and the electronics are turned on. This theory is further reinforced by the fact that a lot of background noise was present at the time of measurement and frequent malfunctions of the electronics were experienced when the data was collected, virtually rendering many readings unusable for research purpose. In order to avoid this in the future all electronic equipment used, should further be tested or replaced in order to make sure everything works properly and that the noise present does not affect the accuracy of the measurements. Helium 5.0 along with a liquid nitrogen cold trap were used in this investigation. For the case of gas purity being a reason for the failed extraction of radon and polonium ions, a higher grade of purity of helium can be used to make sure impurities are not preventing the ions of interest from being extracted. It could also be the case of helium not being the best inert gas for this type of extraction at room temperature, so it is advisable as well to try out with different inert gases (possibly of the highest purity available). An inert gas purification apparatus made up of water and oxygen filters could also be inserted in the gas line as well as adopting longer bake out times ahead of measurement to further help improve the purity of the inert gas used for the extraction. Although the obtained results, do not definitively point to the efficient extraction of all the ions of interest, they supply many hints. This comes as a useful staring point for thinking about

possible future adjustments that need to be made in order to successfully optimize the extraction of ions from gas catcher to ready them for direct mass measurements.

Acknowledgements

Thank you Lisa and Julia for all the help that you gave me in the lab. Big thanks to my parents for supporting me throughout my degree and a big thank you to my friends for being there for me and cheering me up. E grazie a Leo per esser riuscito a finire il tuo corso di studi, nonostante tutte le difficoltà.

References

[1] B. Anđelić. *Direct mass measurements of No, Lr and Rf isotopes with SHIPTRAP and developments for chemical isobaric separation*. PhD thesis, University of Groningen, 7 2021.

[2] A. Mollaebrahimi, B. Anđelić, J. Even, M. Block, M. Eibach, F. Giacoppo, N. Kalantar-Nayestanaki, O. Kaleja, H. R. Kremers, M. Laatiaoui, and S. Raeder. A setup to develop novel Chemical Isobaric SEparation (CISE). *Nuclear Instruments and Methods in Physics Research, Section B: Beam Interactions with Materials and Atoms*, 463:508–511, 1 2020.

[3] J. Even, X. Chen, A. Soylu, P. Fischer, A. Karpov, V. Saiko, J. Saren, M. Schlaich, T. Schlathölter, L. Schweikhard, J. Uusitalo, and F. Wienholtz. The NEXT Project: Towards Production and Investigation of Neutron-Rich Heavy Nuclides. *Atoms*, 10(2):59, 6 2022.

[4] I. Pohjalainen. *Gas-phase chemistry, recoil source characterization and in-gas-cell resonance laser ionization of actinides at IGISOL*. PhD thesis, University of Jyväskylä, 6 2018.

[5] D. J. Morrissey, G. Bollen, M. Facina, and S. Schwarz. Pulsed extraction of ionization from helium buffer gas. *Nuclear Instruments and Methods in Physics Research, Section B: Beam Interactions with Materials and Atoms*, 266(21):4822–4828, 11 2008.

[6] B. D. Hartigan. A Pressure Logging And Control System For the Chemical Isobaric Separation Project, Bachelor thesis, University of Groningen, 7 2020.

[7] J. B. Neumayr, L. Beck, D. Habs, S. Heinz, J. Szerypo, P. G. Thirolf, V. Varentsov, F. Voit, D. Ackermann, D. Beck, M. Block, Z. Di, S. A. Eliseev, H. Geissel, F. Herfurth, F. P. Heßberger, S. Hofmann, H. J. Kluge, M. Mukherjee, G. Münzenberg, M. Petrick, W. Quint, S. Rahaman, C. Rauth, D. Rodríguez, C. Scheidenberger, G. Sikler, Z. Wang, C. Weber, W. R. Plaß, M. Breitenfeldt, A. Chaudhuri, G. Marx, L. Schweikhard, A. F. Dodonov, Y. Novikov, and M. Suhonen. The ion-catcher device for SHIPTRAP. *Nuclear Instruments and Methods in Physics Research, Section B: Beam Interactions with Materials and Atoms*, 244(2):489–500, 3 2006.

[8] J. Lehto, C. Fournier, and J. P. Omtvedt. *Basics of nuclear physics and of radiation, detection and measurement*. E-PUB, 1.61 edition, 2 2017.

[9] S. Purushothaman. *Superfluid Helium and Cryogenic Noble Gases as Stopping Media for Ion Catchers*. PhD thesis, University of Groningen, 11 2008.

[10] B. Potet, G. Diaconu, and F. Bouvot. Nucleus Win, NUBASE software, Atomic Mass Data Center at CSNSM, 2 2017.

[11] C. Droese, S. Eliseev, K. Blaum, M. Block, F. Herfurth, M. Laatiaoui, F. Lautenschläger, E. Minaya Ramirez, L. Schweikhard, V. V. Simon, and P. G. Thirolf. The cryogenic gas stopping cell of SHIPTRAP. *Nuclear Instruments and Methods in Physics Research, Section B: Beam Interactions with Materials and Atoms*, 338:126–138, 11 2014.